Inorganic Chemistry

ARTICLE

pubs.acs.org/IC

Oxidation of Zinc−Thiolate Complexes of Biological Interest by Hydrogen Peroxide: A Theoretical Study

Rima Kassim,[†] Christophe Ramseyer,[‡] and Mironel Enescu*[,§]

[†]Centre de Recherche Universitaire de Djibouti (CRUD), University of Djibouti, Avenue Georges Clemenceau, Djibouti

[‡]UTINAM Institute UMR CNRS 6213 and [§]Laboratoire de Chimie Physique et Rayonnements UMR CEA E4, University of Franche-Comté, 16 route de Gray, 25030-Besançon, Cedex, France

Supporting Information

ABSTRACT: Zinc−thiolate complexes play a major structural and functional role in the living cell. Their stability is directly related to the thiolate reactivity toward reactive oxygen species naturally present in the cell. Oxidation of some zinc−thiolate complexes has a functional role, as is the case of zinc finger redox switches. Herein, we report a theoretical investigation on the oxidation of thiolate by hydrogen peroxide in zinc finger cores of CCCC, CCHC, and CCHH kinds containing either cysteine or histidine residues. In the case of the CCCC core, the calculated energy barrier for the oxidation to sulfenate of the complexed thiolate was found to be 16.0 kcal mol^{-1}, which is 2 kcal mol^{-1} higher than that for the free thiolate. The energy barrier increases to 19.3 and 22.2 kcal mol^{-1} for the monoprotonated and diprotonated CCCC cores, respectively. Substitution of cysteine by histidine also induces an increase in the magnitude of the reaction energy barrier: It becomes 20.0 and 20.9 kcal mol^{-1} for the CCCH and CCHH cores, respectively. It is concluded that the energy barrier for the oxidation of zinc fingers is strictly dependent on the type of ligands coordinated to zinc and on the protonation state of the complex. These changes in the thiolate reactivity can be explained by the lowering of the nucleophilicity of complexed sulfur and by the internal reorganization of the complex (changes in the metal−ligand distances) upon oxidation. The next reaction steps subsequent to sulfenate formation are also considered. The oxidized thiolate (sulfenate) is predicted to dissociate very fast: For all complexes, the calculated dissociation energy barrier is lower than 3 kcal mol^{-1}. It is also shown that the dissociated sulfenic acid can interact with a free thiolate to form a sulfur−sulfur (SS) bridge in a reaction that is predicted to be quasi-diffusion limited. The interesting biological consequences of the modulation of thiolate reactivity by the chemical composition of the zinc finger cores are discussed.

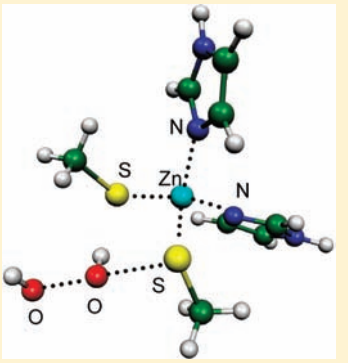

INTRODUCTION

Zinc complexes are prominent components of many classes of proteins and enzymes.[1,2] Their coordination geometry is most often tetrahedral with a combination of cysteine, histidine, glutamate, or aspartate residues as ligands. The thiolate group of cysteine has a particular affinity for Zn^{2+} cation and participates in the active center of enzymes, such as methionine synthase and metalloproteinase.[1] The high affinity of thiolate for zinc allows it to link two zinc centers thus forming metal clusters as in metallothioneins.[3] However, the most abundant protein sites containing zinc are the zinc fingers.[4,5] The term was first used to describe the 30 amino acids binding domain of transcription factor that contains a Cys-Cys-His-His zinc binding motive. Since then, the denomination has been extended to all $Zn(Cys)_\alpha(His)_\beta$, $(\alpha + \beta = 4)$ sites in proteins. For instance, the family of zinc finger proteins also includes the retroviral class (characterized by a Cys-Cys-His-Cys binding motive) and the steroid receptor class (with a Cys-Cys-Cys-Cys binding motive). More often, zinc fingers have a structural role by stabilizing the correct protein folding, but they can also act as active sites or redox switches. A well-known example of a zinc finger acting as an active site is the $Zn(Cys)_4$ core of the DNA repair azodicarbonamide (ADA) protein. The corresponding DNA repairing mechanism assists in the transfer of methyl groups from the DNA backbone phosphoesters to a zinc-complexed cysteine.[6] Redox switches zinc fingers are present in some proteins participating in the cellular defense against the oxidative stress. For instance, bacterial holdase Hsp 33, a chaperone specialized in protecting the proteins against unfolding oxidants, is activated by the oxidation of a $Zn(Cys)_4$ core.[7] The activity of the mammalian Keap 1 protein that regulates the cellular antioxidant response is also modulated by changing the oxidation state of two cysteines in a Cys-Cys-L-L zinc complex (the nature of the ligands L still remains unknown).[8]

In the biological environment, the major part of thiols is carried by the tripeptide glutathione (GSH) whose cellular concentration is of the order of 1 mM. The high GSH concentration will generally protect the functional thiolates in cysteine−zinc complexes against oxidant agents. Obviously, the efficiency of this protection depends on the reactivity of the bound thiolate which may be significantly different with respect to that of free

Received: October 19, 2010
Published: May 20, 2011

Table 1. Gibbs Free Energy Barrier (in kcal mol^{-1}) for the Oxidation of Thiolate and Model Complex $[(MeS)_2(H_2O)_2Zn]$ by H_2O_2 in Aqueous Solution Calculated with Different Computation Methods

	PCM-QCISD(T)/ 6-311+G(2df,2pd)[a]	PCM-B3LYP/ 6-311+G(d,p)	PCM-BMK/ 6-311+G(d,p)	PCM-MPW1PW91/ 6-311+G(d,p)
MeS^-	15.2	10.3	21.0	14.1
$[(MeS)_2(H_2O)_2Zn]$	20.2	16.4	25.0	21.6

[a] Optimization at the PCM-MP2/6-311+G(d,p) level of theory.

thiolate. Indeed, theoretical studies on proton affinity of thiolate in zinc−thiolate complexes showed that the nucleophilicity of thiolate is significantly affected by its coordinative linkage to zinc.[9] The effective strength of zinc−thiolate bond is dependent on the nature of the all four ligands in the complex, as indicated by the variation of the energy barrier for the alkylation of thiolate in various zinc−thiolate complexes.[10]

The protection of zinc-bound thiolates should not be absolute since the oxidation of some of them may play a functional role. This is certainly the case of the redox switches. It was also shown that the zinc complex in matrix metalloproteinases is converted to its active form by the oxidation of the thiolate ligand.[11] Besides, the DNA binding activity of replication protein A (RPA) is regulated through reduction−oxidation of cysteines in a $Zn(Cys)_4$ complex.[12] There is in vitro experimental evidence that thiolate oxidation induces the release of zinc from some metalloproteins,[13,14] and it was suggested that the corresponding in vivo mechanism could be also based on thiolate oxidation. Moreover, in spite of a possible lowering of the reactivity of bound thiolate, it was proposed that the zinc clusters in metallothioneins possess redox activity.[15] It is thus likely that the thiolate environment in zinc−protein complexes confers to it a specific reactivity which preserves the delicate equilibrium between protective and functional requirements.

Obviously, the reactivity of complexed thiolate is fine-tuned by the second sphere molecular interactions, but it is highly dependent on the nature of the ligands participating in the complex. In the present work, we question about the thiolate reactivity with hydrogen peroxide (H_2O_2) in zinc complexes as a function of the type of ligands. Hydrogen peroxide, an important ROS, is a byproduct of normal cell metabolism. The interest for H_2O_2 as an oxidant agent comes from its moderate reactivity allowing it to diffuse over long distances and to reach the less exposed molecular targets. That makes it an efficient agent in signaling the oxidative stress and triggering the zinc finger redox switches.[7,8] Our work is focused on the oxidation of $Zn(Cys)_4$, $Zn(Cys)_3(His)$, and $Zn(Cys)_2(His)_2$ complexes (CCCC, CCHC, and CCHH, respectively) mimicking the zinc finger sites. Since the ligand properties of cysteine are affected by its protonation state, the effect of the cysteine protonation state on the reactivity of these complexes was also considered.

This paper is a first theoretical contribution to the study of the oxidation of zinc complexes of biological interest. The relevance of the reported results depends on the ability of the computation method employed here to provide energy barriers with chemical accuracy (that means expected errors lower than 2 kcal mol^{-1}). We show below that the density functional theory (DFT) with the mPW1PW91[16] functionals predicts energy barriers for the oxidation of free and zinc-complexed thiolates which are very close to those obtained by a post Hartree−Fock method of high level of theory, QCISD(T)[17]/6-311+G(2df,2pd). Hence, by using the mPW1PW91 method, we were able to handle in an efficient manner the large set of reactants, products, and intermediate states involved in the present study without loss in computational accuracy.

COMPUTATIONAL METHOD

State-of-the-art correlated wave function theory is prohibitively expensive to apply to the complex systems of interest here. On the other hand, it was shown that the DFT methods with carefully calibrated exchange and correlation functionals can simultaneously provide accurate barrier heights and binding energies for weakly interacting complexes.[18] After several tests described in the Results Section we chose to use in the present study the mPW1PW91 functionals proposed by Adamo and Barone.[16] All calculations were performed using Gaussian 09 package.[19] Geometries of reactant complexes (RC), product complexes (PC), and transition states (TS) were optimized at the mPW1PW91/6-311+G(d,p) level of theory in aqueous solution. The solvent was treated using the polarizable continuum model (PCM) of Cossi et al.[20] Special attention was paid to the identification of the TSs: Starting geometries were obtained by performing potential energy surface (PES) scans with respect to the main internal coordinates involved in the reaction. Specific TS optimizations were then performed, and the nature of the resulting stationary geometries was checked by frequency calculations. The connection between reactants, TS, and products was checked by performing intrinsic reaction coordinate (IRC) calculations.[21]

The Gibbs free energy in aqueous solution of the stationary state M was calculated as follows:

$$G_{aq}(M) = E_p(M) + \Delta G^{corr}(M) \quad (1)$$

Here $E_p(M)$ is the potential energy calculated by including the PCM solvent contribution, and $\Delta G^{corr}(M)$ represents the thermal and the entropic corrections to Gibbs free energy at T = 298 K and p = 1 atm obtained by frequency calculations in aqueous solution. The reaction energy barriers were calculated as the difference between the Gibbs free energy of the TS and that of the free reactants (FR). It is worth noting that the ΔG^{corr} given by Gaussian 09 is calculated for the standard molar concentration in gas phase. It was corrected for solution phase by adding $RT\ln(c_{0s}/c_{0g})$ (i.e., about 1.8 kcal mol^{-1}), where c_{0s} is the standard molar concentration in aqueous solution, c_{0g} the standard molar concentration in gas phase, and R the gas constant.

For some model systems of smaller size, the Gibbs free energy was also calculated at a high level of the correlated wave function theory in order to test the reliability of the transition-state barriers calculated with the PCM-mPW1PW91/6-311+G(d,p) method. In this reference method, the geometries and ΔG^{corr} were calculated at the PCM-MP2[22]/6-311+G(d,p) level of theory, while the single point potential energy was evaluated at the PCM-QCISD(T)/6-311+G(2df,2pd) level of theory.

Partial atomic charges in the RC, TS, and PC states of different complexes were calculated using the natural population analysis (NPA).[23]

RESULTS

Test of the Computational Method. The performances of three different DFT functionals (B3LYP,[24] BMK,[25] and mPW1PW91) in treating the oxidation of free and complexed thiolate by H_2O_2 were evaluated by comparing the corresponding

Table 2. Main Atomic Distances (in Å) in the TS for the Oxidation of Thiolate and Model Complex $[(MeS)_2(H_2O)_2Zn]$ by H_2O_2 in Aqueous Solution Calculated with Different Computation Methods

	MeS^-		$[(MeS)_2(H_2O)_2Zn]$	
	d(O−O)	d(S^{*b}−O)	d(O−O)	d(S^{*b}−O)
PCM-MP2[a]	1.73	2.39	1.77	2.32
PCM-MPW1PW91[a]	1.74	2.39	1.76	2.29
PCM-BMK[a]	1.77	2.33	1.80	2.25
PCM-B3LYP[a]	1.75	2.46	1.84	2.28

[a] Basis set: 6-311+G(d,p). [b] S* is the attacked sulfur.

energy barriers with those obtained using the high theory level reference method. The thiolate model system was the methanethiolate (MeS^-), while for the complexed thiolate, we considered the model system $[(MeS)_2(H_2O)_2Zn]^{2-}$ where the zinc cation is coordinated by two MeS^- and two water molecules. BMK and mPW1PW91 functionals were chosen because they were specially calibrated for a correct description of reaction energy barriers and of weak interactions involved in the formation of complexes. On the other hand, B3LYP is a very popular hybrid functional providing reasonably good results in a large category of applications. The calculated reaction energy barriers $[G(FR)-G(TS)]$ are given in Table 1. First, one notes that the energy barrier for thiolate oxidation calculated by the reference method is lower by about 1.3 kcal mol^{-1} with respect to the value reported in ref 29 and obtained using a very similar computational method. This deviation arises because the previously reported value was not corrected for the difference between the standard concentrations in gas phase and solution.

It is well-known that the first-generation DFT functionals, such as B3LYP, often underestimate the reaction energy barriers, especially in the case of nucleophilic substitution reactions.[26] This is confirmed by the data listed in Table 1 showing that the B3LYP energy barriers are about 5 and 4 kcal mol^{-1}, respectively, lower than those calculated with the reference method. In spite of its good global performances in predicting reaction energy barriers,[26] the BMK method also fails in the present case. It gives energy barriers for thiolate and complexed thiolate oxidation higher by about 6 and 5 kcal mol^{-1}, respectively, as compared to the reference method. On the other hand, the energy barriers for the present reaction are correctly predicted by the mPW1PW91 method: The corresponding deviations with respect to the reference method are only 1.0 and 1.4 kcal mol^{-1}, respectively (Table 1). A similar agreement between the mPW1PW91 and the reference methods is also observed for molecular geometries. The main atomic distances in the TS state calculated at the MP2 (for the reference method), mPW1PW91, BMH, and B3LYP levels of theory are given in Table 2. The root-mean-square deviation (rmsd) of the mPW1PW91 values with respect to the reference (MP2) values is only 0.016. For the two others methods it is significantly higher: 0.052 Å for the BMK method and 0.054 Å for the B3LYP method.

To the best of our knowledge, the experimental energy barrier for thiolate oxidation by H_2O_2 was not yet reported. We know however that the related experimental reaction rate constant is situated in the 17.0−26.0 mol^{-1} dm^3 s^{-1} range.[27,28] In the TS theory, the reaction rate constant (k) and the reaction energy barrier ($\Delta G^{\ddagger}$) are related by[29]

$$k = (KT/h)\exp(-\Delta G^{\ddagger}/RT) \quad (2)$$

where K is the Boltzmann constant, h is the Planck constant, T is the absolute temperature, and R is the gas constant. This allows us to evaluate an "experimental" reaction energy barrier of about 15.9 kcal mol^{-1}. This value is close to the theoretical value calculated using our reference method. One concludes that the mPW1PW91 method predicts energy barriers for the oxidation of free and complexed thiolate with an expected error lower than 2 kcal mol^{-1}, i.e., with chemical accuracy. In the following, all results will be produced with the mPW1PW91 method.

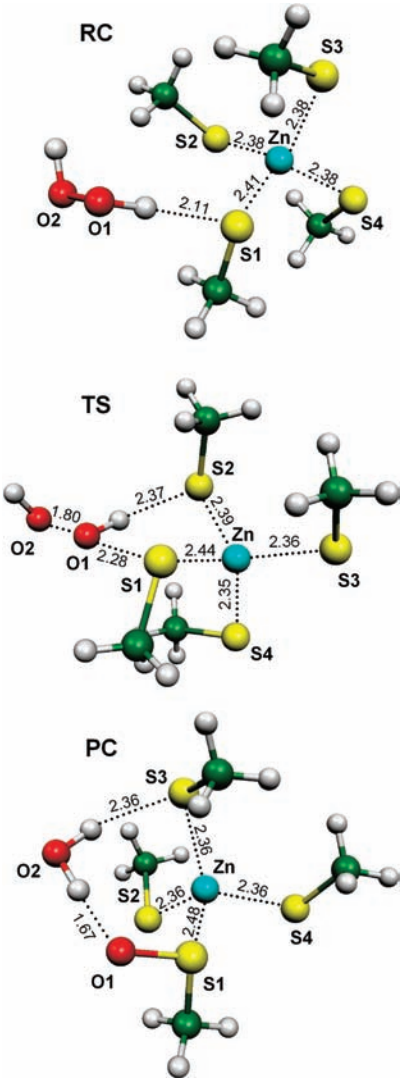

Figure 1. Oxidation of $[(MeS)_4Zn]^{2-}$ by H_2O_2: images of RC, TS, and PC optimized at the PCM-mPW1PW91/6-311+G(d,p) level of theory. The RC and the PC structures were obtained from the TS structure by performing reverse and, respectively, forward IRC calculations then by reoptimizing the two extreme IRC structures.

Oxidation of the CCCC Complex. The protonation state of cysteine in zinc finger complexes is still a matter of debate. Extended X-ray absorption fine structure (EXAFS) measurements on zinc finger models are consistent with all deprotonated thiol configuration.[30,31] This result was recently confirmed by circular dichroism (CD) spectroscopy applied to small peptides

dx.doi.org/10.1021/ic200267x |Inorg. Chem. 2011, 50, 5407–5416

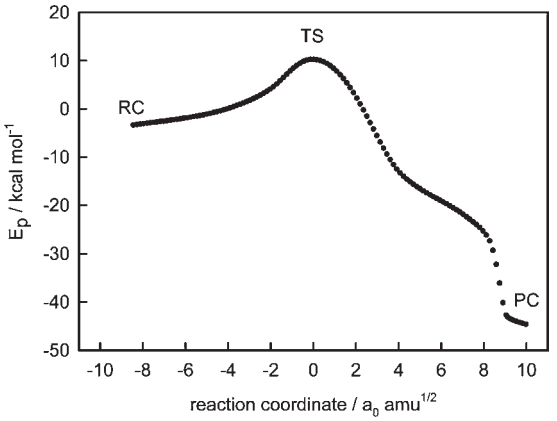

Figure 2. Oxidation of the $[(MeS)_4Zn]^{2-}$ complex by H_2O_2: IRC curve calculated at the PCM-mPW1PW91/6-311+G(d,p) level of theory.

models of CCHH, CCHC, and CCCC type.[32] On the other hand, accurate electrospray mass spectroscopy experiments on a series of consensus zinc finger peptides indicated that, for the three types of complexes that were studied (CCCC, CCHC, or CCHH), only two cysteines were deprotonated.[33] This apparent disagreement could, eventually, be explained by the major effect of the protein environment on the cysteine protonation state.[34] Hence, in the present work we considered three different protonation states of CCCC: the fully deprotonated and the mono- and the diprotonated states. The fully deprotonated CCCC was represented by the model complex $[(MeS)_4Zn]^{2-}$, while the mono- and the diprotonated forms were mimicked by the model systems $[(MeS)_3(MeSH)Zn]^-$ and $[(MeS)_2(MeSH)_2Zn]$, respectively. In the present notation MeSH represents the methanethiol.

The mechanism of thiolate oxidation by hydrogen peroxide was already reported by our group:[29] It consists of a nucleophilic substitution of one oxygen in H_2O_2 by sulfur followed by a hydrogen atom transfer. The reaction products are a sulfenate anion and a water molecule:

$$RS^- + H_2O_2 \rightarrow RSO^- + H_2O \qquad (3)$$

In the case of thiolate−zinc complexes, the thiolate oxidation is expected to be affected either by the lower nucleophilicity of the complexed thiolate or by the internal reorganization of the zinc complex (changes in the metal−ligand distances) following this oxidation.

PES scan of the $H_2O_2/[(MeS)_4Zn]^{2-}$ system with respect to the S−O and O−O distances allowed us to detect three stationary structures (Figure 1): a RC, a TS, and a PC. The imaginary frequency in TS belongs to a normal mode that is a combination of the S−O and O−O distances. IRC calculations (Figure 2) demonstrate that the three structures here identified (RC, TS, and PC) are directly connected. Practically, we have first identified the TS, then we performed reverse and, respectively, forward IRC calculations. The last structure in the reverse IRC trajectory was then reoptimized to get the RC structure. The PC structure was obtained in a similar way. This procedure was applied to all the complexes studied in the present work. The evolution of the RC complex to the PC complex via the TS, as described by the IRC curve in Figure 2, is a nucleophilic substitution of O2 atom by the S1 atom followed by a hydrogen atom transfer. The hydrogen atom transfer is indicated on the IRC curve by the shoulder appearing at about 8 $a_0 \cdot amu^{1/2}$ (here a_0 is the Bohr radius). We conclude that the reaction mechanism of thiolate oxidation by H_2O_2 in the $[(MeS)_4Zn]^{2-}$ complex is similar to that observed for the oxidation of free thiolate.[29] However, a careful comparison of stationary structures involved in the two processes reveals some specific differences. First of all, the TS conformations are not identical (Table 3): the S*−O distance (S* is the attacked sulfur) is shorter in the case of complex (2.28 Å as compared to 2.39 Å obtained for free thiolate), while the O−O distance is longer (1.80 Å as compared to 1.74 Å for free thiolate). One notes also that the TS for the oxidation of $[(MeS)_4Zn]^{2-}$ is supplementary stabilized by a hydrogen bond formed between H(O1) and S2 (Figure 1). Different starting configurations for the optimization of the TS led to the same final structure. We conclude that the TS in Figure 1 is the only one possible for this complex.

The internal reorganization of the complex during this reaction is emphasized by the evolution of the S−Zn bonds length. The S−Zn bonds of the free complex (not shown) are all equivalent, and their common length is 2.38 Å. The equivalence of the bonds is lost even in the RC state where the S−Zn bond lengths vary between 2.38 and 2.41 Å. Interestingly, in the PC state the oxidized sulfur is not completely released, but its distance with respect to zinc increases at 2.48 Å. At the same time, the S−Zn bonds of inactive thiolates become tighter as shown by their lengths stabilized at about 2.36 Å. Since thiolate oxidation is associated with a significant redistribution of the electric charge between the active atoms (denoted by S1, O1, and O2 in Figure 1), one could expect the electric charge on Zn and the three other sulfur atoms to be also affected. The natural atomic charges calculated for the RC, TS and PC states are given in Table 4. According to the present results, a negative charge of about one electron is transferred during oxidation from S1 to O1 and O2, but the zinc and the three remaining sulfur atoms do not practically participate to the charge redistribution. The absence of charge redistribution between ligands indicates that sulfenate has a nucleophilic activity comparable to that of thiolate.

The result of all these specific interactions is a modest rise of the TS barrier from 14.1 kcal mol^{-1}, that is the barrier for the oxidation of free thiolate, to 16.0 kcal mol^{-1} (see G_{aq}(TS) in Table 5).

Protonation of one or two thiolates significantly affects the interaction between the metal and the four ligands. This is clearly shown by the changes in the S−Zn distances. For thiolate, this distance decreases from 2.38 Å in $[(MeS)_4Zn]^{2-}$ to 2.31 and 2.29 Å in $[(MeS)_3(MeSH)Zn]^-$ and $[(MeS)_2(MeSH)_2Zn]$, respectively. For thiol, it is 2.67 Å in $[(MeS)_3(MeSH)Zn]^-$ and 2.57 Å in $[(MeS)_2(MeSH)_2Zn]$. The mechanism of thiolate oxidation is preserved. It consists of a S→O nucleophilic substitution followed by a hydrogen atom transfer (Figures 3 and 4 for $[(MeS)_2(MeSH)_2Zn]$ and Figures 1s and 2s in the Supporting Information for $[(MeS)_3(MeSH)Zn]^-$). The hydrogen atom transfer occurs for a value of the reaction coordinate of about 5 $a_0 \cdot amu^{1/2}$ (Figure 4) that is significantly earlier as compared to the oxidation of $[(MeS)_4Zn]^{2-}$. The geometry of the TS is highly sensitive to the protonation state of the complex (Table 3): the S*−O distance decreases from 2.28 Å in the fully deprotonated complex to 2.22 Å in the monoprotonated and to 2.18 Å in the diprotonated complex. Conjointly, the O−O distance increases from 1.80 Å to 1.83 and 1.86 Å, respectively. But the most spectacular result is the rise of the reaction energy barrier with respect to the fully deprotonated case by 3.3 kcal mol^{-1} for $[(MeS)_3(MeSH)Zn]^-$ and by 8.0 kcal mol^{-1} for

dx.doi.org/10.1021/ic200267x |*Inorg. Chem.* 2011, 50, 5407–5416

Table 3. Main Atomic Distances (in Å) in the TS for the Oxidation of the Free and Zinc-Complexed Methanethiolate by H_2O_2 in Aqueous Solution Calculated at the PCM-mPW1PW91/6-311+G(d,p) Level of Theory

	d(Zn−S*)[a]	d(Zn−S)	d(Zn−S(H))	d(O−O)	d(S*[a]−O)
MeS^-	–	–	–	1.74	2.39
$[(MeS)_4Zn]^{2-}$	2.44	2.35	–	1.80	2.28
$[(MeS)_3(MeSH)Zn]^-$	2.39	2.31	2.62	1.83	2.22
$[(MeS)_2(MeSH)_2Zn]$	2.36	2.29	2.51	1.86	2.18
$[(MeS)_3(Im)Zn]^-$	2.41	2.33	–	1.80	2.26
$[(MeS)_2(MeSH)(Im)Zn]$	2.35	2.28	2.59	1.82	2.22
$[(MeS)_2(Im)_2Zn]$	2.36	2.31	–	1.80	2.25

[a] S* is the attacked sulfur.

Table 4. Evolution of Main Natural Atomic Charges during the Oxidation of CCCC Complexes Calculated with the NPA Method at the PCM-mPW1PW91/6-311+G(d,p) Level of theory

	$[(MeS)_4Zn]^{2-}$			$[(MeS)_3(MeSH)Zn]^-$			$[(MeS)_2(MeSH)_2Zn]$		
	RC	TS	PC	RC	TS	PC	RC	TS	PC
O	−0.49	−0.80	−1.04	−0.49	−0.83	−1.01	−0.49	−0.88	−1.0
O(S)	−0.53	−0.65	−1.09	−0.52	−0.66	−1.01	−0.52	−0.66	−1.07
S(O)	−0.50	−0.15	0.56	−0.49	−0.09	0.59	−0.47	−0.05	0.60
S	−0.54	−0.52	−0.53	−0.51	−0.50	−0.51	−0.50	−0.49	−0.49
S(H)	–	–	–	0.01	0.02	0.01	0.02	0.04	0.02
Zn	0.64	0.63	0.60	0.70	0.70	0.70	0.76	0.76	0.75

Table 5. Gibbs Free Energy of the Stationary States Involved in the Oxidation of Several Zinc Complexes by H_2O_2 in Aqueous Solution

	G_{aq}(RC)[a]	G_{aq}(TS)[a]	G_{aq}(TS′)[a]	G_{aq}(PC)[a]
$[(MeS)_4Zn]^{2-}$	2.8	16.0	–	−40.0
$[(MeS)_3(MeSH)Zn]^-$	2.2	19.3	22.3	−33.5
$[(MeS)_2(MeSH)_2Zn]$	5.8	24.0	22.2	−31.1
$[(MeS)_3(Im)Zn]^-$	2.5	21.4	20.0	−39.2
$[(MeS)_2(MeSH)(Im)Zn]$	4.1	22.4	22.5	−33.2
$[(MeS)_2(Im)_2Zn]$	3.8	20.9	21.7	−36.3

[a] In kcal mol^{-1}; reference: the free reactants state.

$[(MeS)_2(MeSH)_2Zn]$ (Table 5). In fact, a comparison of the data in Tables 3 and 5 indicates that the energy barrier height and the S*−O distance in the TS are well correlated: A shorter S*-O distance is associated with a higher energy barrier.

The loss in the symmetry of the complex due to thiolate protonation makes possible alternative transition states in the case of the $[(MeS)_3(MeSH)Zn]^-$ and $[(MeS)_2(MeSH)_2Zn]$ complexes (Figures 3s in the Supporting Information and 5, respectively). These alternative transition states denoted TS′ are not perturbed by hydrogen bonds and were obtained by choosing a way of attack to sulfur passing between a thiol and a thiolate. Interestingly, for $[(MeS)_3(MeSH)Zn]^-$ the energy barrier related to the TS′ state is higher by 3 kcal mol^{-1} with respect to the former one, while for $[(MeS)_2(MeSH)_2Zn]$ it is lower by 1.8 kcal mol^{-1} (Table 5). This shows that the hydrogen-bonding effect is complex, and it is not always a stabilizing factor for the transition state. When the lowest transition states are considered, the increase in the magnitude of the oxidation energy barrier upon protonation is 3.3 kcal mol^{-1} for $[(MeS)_3(MeSH)Zn]^-$ and 6.2 kcal mol^{-1} for $[(MeS)_2(MeSH)_2Zn]$. One notes also that, as in the case of $[(MeS)_4Zn]^{2-}$, the thiolate oxidation does not induce any relevant electronic redistribution on zinc and the three inactive sulfur ligands (Table 5).

The main conclusion to be retained from these results is that the thiolate reactivity with H_2O_2 in the CCCC zinc finger cores is strongly dependent on the protonation state of the complex.

Oxidation of the CCHC and CCHH Complexes. Zinc-finger sites CCHC and CCHH were mimicked by the model systems $[(MeS)_3(Im)Zn]^-$ and $[(MeS)_2(Im)_2Zn]$, respectively, where Im signifies imidazole. In the case of the CCHC site, the monoprotonated form $[(MeS)_2(MeSH)(Im)Zn]$ was also considered. The diprotonated form of CCHC site and the monoprotonated form of the CCHH site were disregarded because, as shown by Fabris et al.,[33] for the thermodynamic stability of these kinds of complexes at least two deprotonated cysteines are required as ligands.

Substitution of one or two thiolates in $[(MeS)_4Zn]^{2-}$ by Im affects the interaction between zinc and the remaining sulfur ligands: The S−Zn distances decrease from 2.38 Å (in the all-thiolate complex) to 2.34 Å in $[(MeS)_3(Im)Zn]^-$ and to 2.31 Å in $[(MeS)_2(Im)_2Zn]$. These variations are less important as compared to those induced upon thiolate substitution by thiol, suggesting that imidazole is a better ligand for zinc than thiol. Although the mechanism of thiolate oxidation in the Im substituted complexes is very similar to that observed in the case of $[(MeS)_4Zn]^{2-}$ (Figure 6−10), some variations in the hydrogen-bond patterns from one species to another are present. For instance, the reactant complex is stabilized by a hydrogen bond between O1 and the Im ring in the case of $[(MeS)_3(Im)Zn]^-$ (Figure 6) and by two hydrogen bonds in the case of $[(MeS)_2(Im)_2Zn]$. The latter hydrogen bonds involve the O1 and the O2 atoms, respectively, and the two Im rings (Figure 9). The ImCH···O1 hydrogen bonds are preserved in the TSs of both

dx.doi.org/10.1021/ic200267x |Inorg. Chem. 2011, 50, 5407–5416

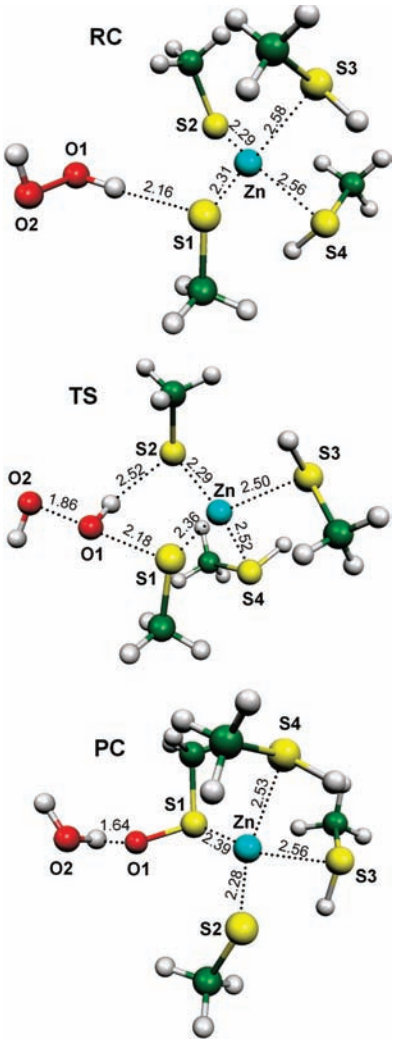

Figure 3. Oxidation of $[(MeS)_2(MeSH)_2Zn]$ by H_2O_2: Images of RC, TS, and PC optimized at the PCM-mPW1PW91/6-311+G(d,p) level of theory. The RC and the PC structures were obtained from the TS structure by performing reverse and, respectively, forward IRC calculations then by reoptimizing the two extreme IRC structures.

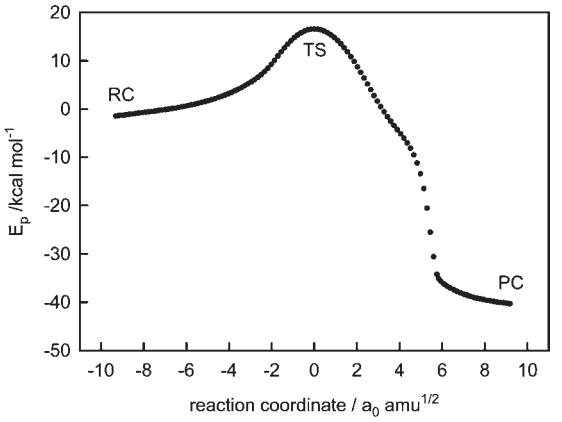

Figure 4. Oxidation of $[(MeS)_2(MeSH)_2Zn]$ by H_2O_2: IRC curve calculated at the PCM-mPW1PW91/6-311+G(d,p) level of theory.

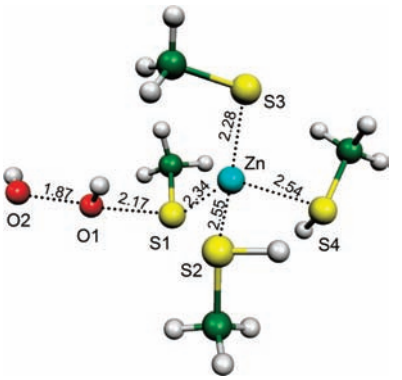

Figure 5. Oxidation of $[(MeS)_2(MeSH)_2Zn]$ by H_2O_2: Image of the TS′ optimized at the PCM-mPW1PW91/6-311+G(d,p) level of theory.

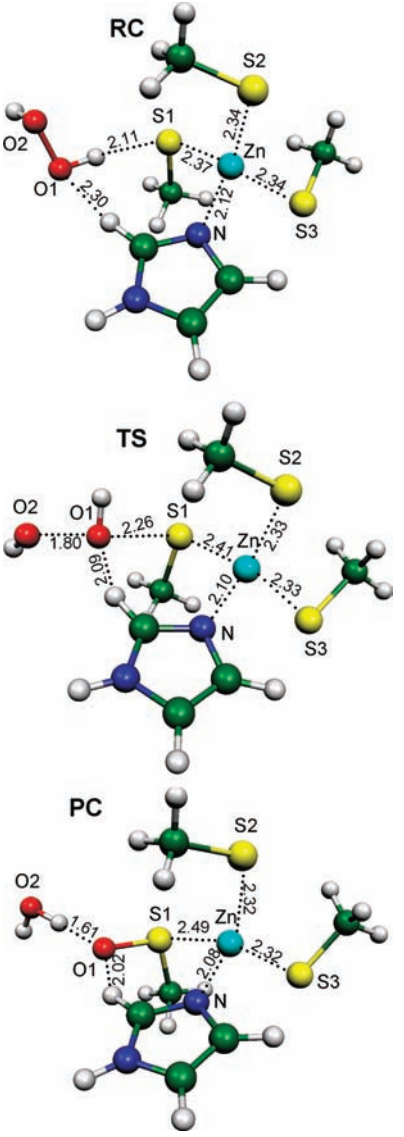

Figure 6. Oxidation of $[(MeS)_3(Im)Zn]^-$ by H_2O_2: Images of RC, TS, and PC optimized at the PCM-mPW1PW91/6-311+G(d,p) level of theory. The RC and the PC structures were obtained from the TS structure by performing reverse and, respectively, forward IRC calculations then by reoptimizing the two extreme IRC structures.

dx.doi.org/10.1021/ic200267x |*Inorg. Chem.* 2011, 50, 5407–5416

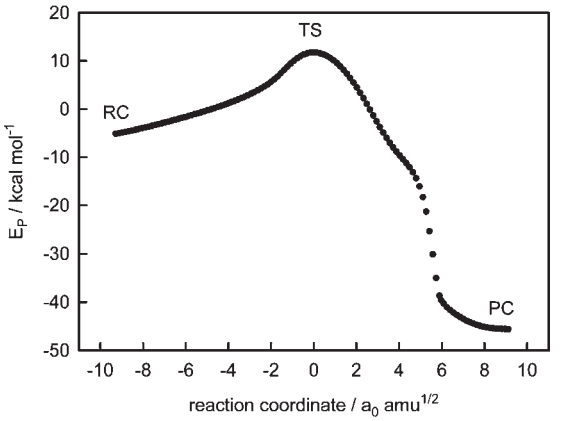

Figure 7. Oxidation of $[(MeS)_3(Im)Zn]^-$ by H_2O_2: IRC curve calculated at the PCM-mPW1PW91/6-311+G(d,p) level of theory.

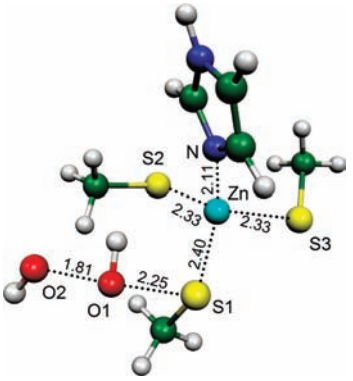

Figure 8. Oxidation of $[(MeS)_3(Im)Zn]^-$ by H_2O_2: Image of TS′ optimized at the PCM-mPW1PW91/6-311+G(d,p) level of theory.

systems, while the ImCH···O2 bond, present in the RC state of $[(MeS)_2(Im)_2Zn]$, is transferred to the Im ring already bound to O1. The overall internal reorganization in the TS of the two complexes is resumed in Table 3. The most significant variation occurs on the Zn−S* distance: It changes from 2.34 to 2.41 Å for $[(MeS)_3(Im)Zn]^-$ and from 2.31 to 2.36 Å for $[(MeS)_2(Im)_2Zn]$. It is obvious that, given the complexity of the systems, the configuration of the RC complex is not uniquely determined. However, this has only minor consequences on the reaction kinetics which is mainly dependent on the Gibbs free energy difference between the FR and the TSs.

Given the asymmetry of the $[(MeS)_3(Im)Zn]^-$ and $[(MeS)_2(Im)_2Zn]$ complexes, in both cases a second transition states, TS′, was found by choosing the direction of attack to sulfur to be quasiperpendicular to the plan containing the closest imidazole ring. This conformation does not allow hydrogen bonding between peroxide and imidazole. The corresponding transition states are shown in Figures 8 (for $[(MeS)_3(Im)Zn]^-$) and 11 (for $[(MeS)_2(Im)_2Zn]$). In the case of $[(MeS)_3(Im)Zn]^-$, the S*−O and, respectively, the O−O distances are quite similar in the TS and TS′ states. On the other hand, the Gibbs free energy of the TS′ state is lower by 1.4 kcal mol^{-1} with respect to that of the TS (Table 5). The S*−O and O−O distances in the second transition state of $[(MeS)_2(Im)_2Zn]$ are 2.21 and 1.83 Å, respectively, that are somewhat different with respect to those found for the former

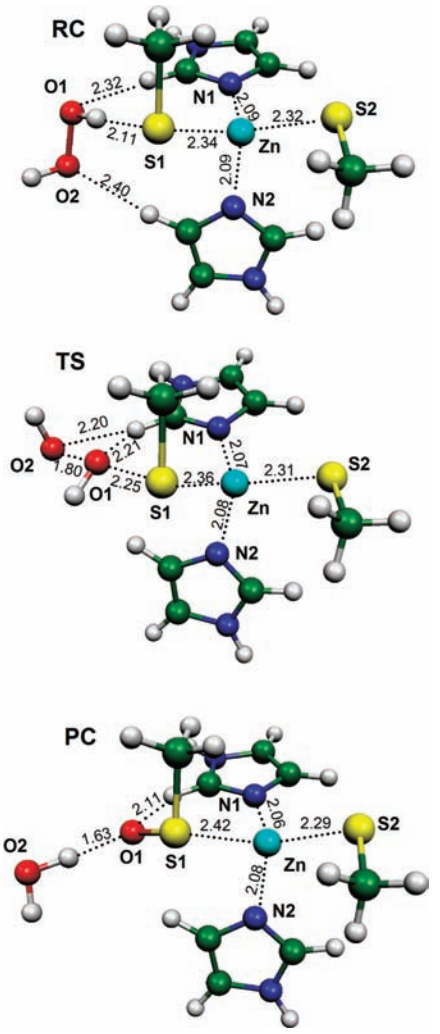

Figure 9. Oxidation of $[(MeS)_2(Im)_2Zn]$ by H_2O_2: Images of RC, TS, and PC optimized at the PCM-mPW1PW91/6-311+G(d,p) level of theory. The RC and the PC structures were obtained from the TS structure by performing reverse and, respectively, forward IRC calculations then by reoptimizing the two extreme IRC structures.

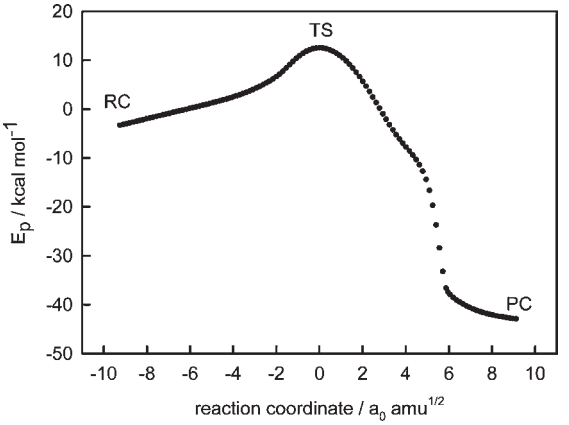

Figure 10. Oxidation of $[(MeS)_2(Im)_2Zn]$ by H_2O_2: IRC curve calculated at the PCM-mPW1PW91/6-311+G(d,p) level of theory.

transition state (Figure 11 and 9, respectively). For this complex, the lowest transition states is the TS, but the difference in Gibbs

dx.doi.org/10.1021/ic200267x |*Inorg. Chem.* 2011, 50, 5407–5416

free energy between the two states is only 0.8 kcal mol^{-1} (Table 5). One notes once again that the hydrogen bonding in the transition state has contradictory effects. On the other hand, when the lowest transition states of the two complexes are compared, $[(MeS)_2(Im)_2Zn]$ appears as slightly less reactive than $[(MeS)_3(Im)Zn]^-$. Both complexes are significantly less reactive than $[(MeS)_4Zn]^{2-}$: Their oxidation energy barriers are 4 kcal mol^{-1} (for $[(MeS)_3(Im)Zn]^-$) and 4.9 kcal mol^{-1} (for $[(MeS)_2(Im)_2Zn]$) higher than that calculated for the all-thiolate complex (Table 5).

The protonation effect on the oxidation of mixed thiolate-imidazole zinc complexes was found to be comparable to that observed in the case of $[(MeS)_4Zn]^{2-}$. In the FR state of $[(MeS)_2(MeSH)(Im)Zn]$, the S−Zn distance is 2.60 Å for thiol and only 2.29 Å for the two thiolates (that is 0.05 Å shorter than in $[(MeS)_3(Im)Zn]^-$). Some geometry differences with respect to the case of the unprotonated complex $[(MeS)_3(Im)Zn]^-$ are also observed in the TS (Figure 4s, Supporting Information). The Zn−S* and S*−O distances are shorter by 0.06 and 0.04 Å, respectively. A second transition state, TS′, was found for this complex also (Figure 6s, Supporting Information). While in the TS the peroxide is bound to imidazole by two hydrogen bonds, in the TS′ state no such hydrogen bonds are present. However, the two energy barriers are almost equal (Table 5). When the lowest transition states of the two complexes are compared, the energy barrier for the oxidation of the protonated complex is found to be 2.4 kcal mol^{-1} higher with respect to that calculated for the unprotonated complex.

The evolution of the partial atomic charges during oxidation of $[(MeS)_2(Im)_2Zn]$, $[(MeS)_3(Im)Zn]^-$ and $[(MeS)_2(MeSH)(Im)Zn]$ complexes is very similar to that found for the CCCC complexes: A negative charge of about one electron is transferred from S1 to O1 and O2, while the partial atomic charges on zinc and on the three remaining ligand atoms are practically constant (Tables 4−6).

We conclude that thiolate substitution by imidazole induces a significant increase of the energy barrier for the oxidation of zinc finger model cores by H_2O_2. Further energy barrier rise occurs upon protonation of the remaining thiolates.

Dissociation of the Oxidized Thiolate. Since was experimentally shown that thiolate oxidation in zinc complexes induces zinc release,[13,14] it is expected that the oxidized thiolate dissociates faster than thiolate. We studied this dissociation in the case of three zinc complexes: $[(MeSOH)(MeS)_3Zn]^-$, $[(MeSOH)(MeS)(MeSH)_2Zn]^+$, and $[(MeSOH)(MeS)(Im)_2Zn]^+$. Obviously, these complexes are the oxidized forms of $[(MeS)_4Zn]^{2-}$, $[(MeS)_2(MeSH)_2Zn]$, and $[(MeS)_2(Im)_2Zn]$, respectively. They were chosen for this dissociation study in reason of their significant structural differences. It was assumed that in the oxidized complexes the sulfenate is in its protonated form. In fact, to the best of our knowledge, no reliable experimental data exist for the pK_a value of the sulfenic acid (RSOH). However, corroborated theoretical evaluations strongly suggest a value around 10 (ref 35) that means that at neutral pH the sulfenate will be protonated. Obviously, sulfenate protonation strongly reduces its nucleophilicity.

The dissociation curves were calculated by performing constrained geometry optimizations with S−Zn distance (S belongs to MeSOH) as a constrained coordinate. The results shown in Figure 12 predict a fast dissociation in all cases. Indeed, the potential energy barrier for this process is only 0.3 kcal mol^{-1} for $[(MeSOH)(MeS)(MeSH)_2Zn]^+$, while its highest value is lower than 2.6 kcal mol^{-1} and is obtained for $[(MeSOH)(MeS)(MeSH)_2Zn]^+$.

The dissociated sulfenic acid can then interact with a thiolate to form a disulfide bridge according to the reaction:

$$RSOH^- + R'S^- \rightarrow RSSR' + HO^- \quad (4)$$

The reaction is a nucleophilic substitution. The corresponding transition state calculated for the reaction between the model systems CH_3SOH and CH_3S^- is represented in Figure 13. The reaction is predicted to be quasidiffusion-limited since the corresponding potential energy barrier is lower than 1 kcal mol^{-1} (Figure 14). In the biological environment, the sulfenic acid formed in the first step of a zinc finger oxidation process could in principle react with a second thiolate that is either complexed or dissociated. The process may involve several reaction steps and requires a specific approach that is beyond the aim of the present paper.

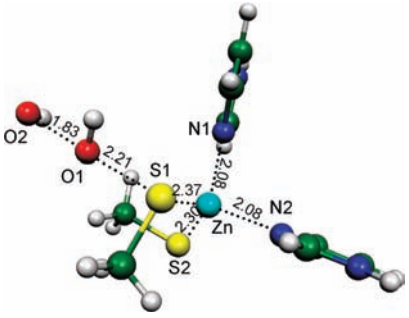

Figure 11. Oxidation of $[(MeS)_2(Im)_2Zn]$ by H_2O_2: Image of TS′ optimized at the PCM-mPW1PW91/6-311+G(d,p) level of theory.

DISCUSSION

The present theoretical study confirms that the thiolate complexation to zinc in zinc finger cores reduces its reactivity

Table 6. Evolution of Main Natural Atomic Charges during the Oxidation of CCHC and CCHH Complexes Calculated with the NPA Method at the PCM-mPW1PW91/6-311+G(d,p) Level of Theory

	$[(MeS)_3(Im)Zn]^-$			$[(MeS)_2(MeSH)(Im)Zn]$			$[(MeS)_2(Im)_2Zn]$		
	RC	TS	PC	RC	TS	PC	RC	TS	PC
O	−0.48	−0.79	−1.02	−0.48	−0.81	−1.00	−0.48	−0.79	−1.01
O(S)	−0.53	−0.63	−1.08	−0.52	−0.63	−1.07	−0.52	−0.63	−1.07
S(O)	−0.48	−0.12	0.57	−0.47	−0.08	0.59	−0.47	−0.11	0.58
S	−0.52	−0.51	−0.51	−0.49	−0.50	−0.50	−0.51	−0.51	−0.50
S(H)	–	–	–	0.02	0.02	0.02	–	–	–
N(Zn)	−0.60	−0.61	−0.61	−0.63	−0.64	−0.64	−0.61	−0.61	−0.62
Zn	0.77	0.78	0.75	0.86	0.88	0.85	0.93	0.96	0.92

dx.doi.org/10.1021/ic200267x |*Inorg. Chem.* 2011, 50, 5407–5416

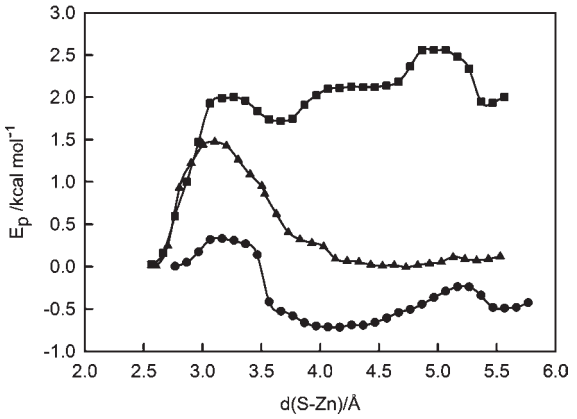

Figure 12. Potential energy curves for the dissociation of the oxidized thiolate (CH_3SOH) from the oxidized zinc complexes: $[(MeSOH)(MeS)_3Zn]^-$(solid circles, ●), $[(MeSOH)(MeS)(MeSH)_2Zn]^+$(solid squares, ■), and $[(MeSOH)(MeS)(Im)_2Zn]^+$(solid triangles,▲). The curves were calculated at the PCM-mPW1PW91/6-311+G(d,p) level of theory.

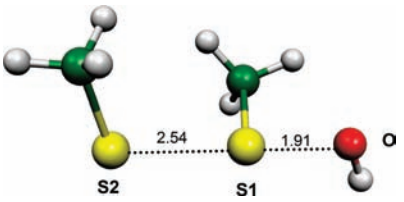

Figure 13. SS bridge formation: The TS for the reaction between CH_3S^- and CH_3SOH calculated at the PCM-mPW1PW91/6-311+G(d,p) level of theory.

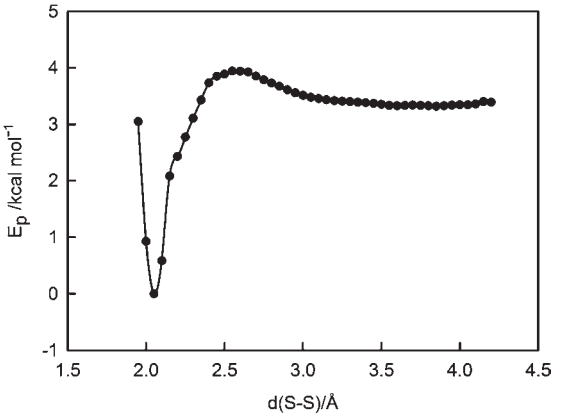

Figure 14. SS bridge formation: Potential energy scan with respect to the S−S distance for the reaction between CH_3S^- and CH_3SOH. The curve was calculated at the PCM-mPW1PW91/6-311+G(d,p) level of theory.

with H_2O_2. The corresponding rise of the energy barrier was determined with chemical accuracy. It is situated between 2 and 8 kcal mol^{-1}, depending on the chemical composition of the complex. According to eq 2, this implies a decrease in the reaction rate constant by a factor of 30 to 2 × 10^6, which is significant for the redox equilibrium of thiolate.

Looking for a general reactivity trend in the series of complexes here analyzed, one could propose, as Picot et al.[10] already did for the alkylation reaction, that in zinc finger complexes the reactivity decreases when the negative charge of the complex decreases. In our case, this is strictly true for the CCCC complex and its differently protonated states. This is true also for the substitution of thiolate by imidazole, as can be seen by comparing the oxidation energy barriers of $[(MeS)_4Zn]^{2-}$, $[(MeS)_3(Im)Zn]^-$, and $[(MeS)_2(Im)_2Zn]$ (Table 5). Consequently, the reactivity trend experimentally observed for the alkylation reaction,[36] i.e., free thiolate > $(thiolate)_4Zn$ > $(thiolate)_3(Im)Zn$ > $(thiolate)_2(Im)_2Zn$, is respected for the oxidation too. On the other hand, on notes that, although $[(MeS)_2(MeSH)_2Zn]$ and $[(MeS)_2(Im)_2Zn]$ are both electrically neutral, their reactivities are significantly different. This shows that the charge of the complex is not the only one parameter relevant for the reactivity of the complex.

The difficulty in rationalizing these results also comes from the fact that the reaction energy barrier is dependent not only on the nucleophilicity of the complexed sulfur, but also on the internal reorganization of the complex in the transition state. This internal reorganization consists in a shortening of the distances between metal and the not reacting ligands. On the other hand, given the fact that the energy barriers for five of the six complexes here considered is spread over a range of 3 kcal mol^{-1} only, further analysis is not really very relevant. The main conclusions to be retained are: (i) The reactivity of the CCCC complex with H_2O_2 decreases significantly upon protonation; and (ii) the mixed thiolate-imidazole zinc complexes have oxidation energy barriers that are greater by about 4−6 kcal mol^{-1} with respect to that of the fully deprotonated CCCC complex and that are less sensitive to the detailed chemical composition of the complex.

The first of these two findings has a very interesting biological significance. It shows that the thiolate reactivity in the CCCC complexes can be efficiently modulated by changing the protonation state of the complex. This is naturally possible because the cysteine pK_a is sensitive to the protein environment. For instance, Sénèque and Latour[32] have reported variations of cysteine pK_a in CCCC zinc finger sites of about 2 units. One can further infer that the CCCC sites whose oxidation presents a functional role (as is the case of redox switches) adopt, very likely, a fully deprotonated state. The other CCCC sites need a specific protection against reaction with the hydrogen peroxide. This protection can by acquired by protonation or by electrostatic screening provided by the protein environment. Indeed, the analysis performed by Maynard and Covell[34] on 207 zinc finger cores revealed that, among them, the electrostatic screening is maximum for the CCCC cores.

The small decrease of the thiolate reactivity in the fully deprotonated CCCC complex means that, in this case, the thiolate preserves its antioxidant properties. Hence, it could play an antioxidant role in the living cell, as was already proposed for the thiolate in the metallothionein zinc clusters.[15] However, in the case of metallotionein, a more specific theoretical analysis is necessary before concluding about the reactivity of its thiolates. Indeed, our calculations predict a high sensibility of the thiolate reactivity with respect to zinc coordination that is not identical in metallotnionein and CCCC cores. Some thiolates in the metallothionein zinc clusters are linked to two metal centers.

In the present analysis we have considered the thiolate reactivity only in relation with the chemical composition of the zinc finger cores. Obviously, a second factor affecting this reactivity is the protein environment. For instance, it was already shown that the energy barrier for the thiolate oxidation by H_2O_2 is very sensitive to the dielectric constant of the environment.[29]

dx.doi.org/10.1021/ic200267x |*Inorg. Chem.* 2011, 50, 5407–5416

The PCM model using the dielectric constant of water is expected to give a realistic description of the solvent interaction only in the case of the solvent exposed zinc finger. Protein environment effects could be mimicked at the same level of theory by using dielectric constant values lower than 80, according to the degree of zinc finger exposure to the solvent. More specific interactions, such as polar group interactions[37] or hydrogen bonding,[10] can also affect the thiolate reactivity. Hence, in the real environment, these interactions could significantly modulate the effects of the chemical composition. This will be investigated in future studies.

CONCLUSION

The energy barrier for the oxidation of thiolate by H_2O_2 in zinc finger complexes is significantly dependent on the type of ligands coordinated to zinc and the protonation state of the complex. This energy barrier can be further modulated by secondary interactions with the protein environment. The conjugation of these factors allows, in principle, a fine-tuning of the zinc fingers reactivity according to their functions. A lower reactivity can be achieved for structural or enzymatic zinc fingers and a higher one for the zinc finger involved in the cellular defense against the oxidative stress (the redox switches or the zinc fingers possessing antioxidant function).

ASSOCIATED CONTENT

Supporting Information. Gaussian 09 input files containing the optimized structures of all the TSs here reported and the stationary structures and IRC curves for the oxidation of $[(MeS)_3(MeSH)Zn]^-$ and $[(MeS)_2(MeSH)(Im)Zn]$. This material is available free of charge via the Internet at http://pubs.acs.org.

AUTHOR INFORMATION

Corresponding Author

*E-mail: mironel.enescu@univ-fcomte.fr. Telephone: 00 33 (0) 3 81 66 65 21.

ACKNOWLEDGMENT

Present calculations were carried out largely on the supercomputer facility at the Mésocentre, a regional computational center at the University of Franche-Comté. One of the authors thanks the Ministère des Affaires Etrangères (MAE) for financial supports through the EMRAUD program.

REFERENCES

(1) Parkin, G. *Chem. Rev.* **2004**, *104*, 699–767.
(2) Maret, W. *Biochemistry* **2004**, *43*, 3301–3309.
(3) Chan, J.; Huang, Z.; Merrifield, M. E.; Salgado, M. T; Stillman, M. J. *Coord. Chem. Rev.* **2002**, *233−234*, 319–339.
(4) Andreini, A.; Banci, L.; Bertini, I.; Rosato, A. *J. Proteome Res.* **2006**, *5*, 196–201.
(5) Lachenmann, M. J.; Ladbury, J. E.; Dong, J.; Huang, K.; Carey, P.; Weiss, M. A. *Biochemistry* **2004**, *43*, 13910–13925.
(6) Myers, L. C.; Jackow, F.; Verdine, G. L. *J. Biol. Chem.* **1995**, *270*, 6664–6670.
(7) Kumsta, C; Jakob, U. *Biochemistry* **2009**, *48*, 4666–4676.
(8) Dinkova-Kostova, A. T.; Holtzclaw, W. D.; Wakabayashi, N. *Biochemistry* **2005**, *44*, 6889–6899.
(9) Ohanessian, G.; Picot, D.; Frison, G. *Int. J. Quantum Chem.* **2011**, *111*, 1239–1247.
(10) Picot, D.; Ohanessian, G.; Frison, G. *Inorg. Chem.* **2008**, *47*, 8167–8178.
(11) H. Nagasse, H.; Woessner, J. F., Jr. *J. Biol. Chem.* **1999**, *274*, 21491–21494.
(12) You, J.-S.; Wang, M.; Lee, S.-H. *Biochemistry* **2000**, *39*, 12953–12958.
(13) Jiang, L.-J.; Maret, W.; Vallee, B. L. *Proc. Natl. Acad. Sci. U.S.A.* **1998**, *95*, 3483–3487.
(14) Korichneva, I.; Hoyos, B.; Chua, R.; Levi, E.; Hammerling, U. *J. Biol. Chem.* **2002**, *277*, 44327–44331.
(15) Maret, W.; Vallee, B. L. *Proc. Natl. Acad. Sci. U.S.A.* **1998**, *95*, 3478–3482.
(16) Adamo, C.; Barone, V. *J. Comput. Chem.* **1998**, *19*, 418–429.
(17) Pople, J. A.; Head-Gordon, M.; Raghavachari, K. *J. Chem. Phys.* **1987**, *87*, 5968–5975.
(18) Zhao, Y.; Truhlar, D. H. *J. Phys. Chem. A* **2005**, *109*, 5656–5667.
(19) Frisch, M. J.; Trucks, G. W.; Schlegel, H. B.; Scuseria, G. E.; Robb, M. A.; Cheeseman, J. R.; Scalmani, G.; Barone, V.; Mennucci, B.; Petersson, G. A.; Nakatsuji, H.; Caricato, M.; Li, X.; Hratchian, H. P.; Izmaylov, A. F.; Bloino, J.; Zheng, G.; Sonnenberg, J. L.; Hada, M.; Ehara, M.; Toyota, K.; Fukuda, R.; Hasegawa, J.; Ishida, M.; Nakajima, T.; Honda, Y.; Kitao, O.; Nakai, H.; Vreven, T.; Montgomery, Jr., J. A.; Peralta, J. E.; Ogliaro, F.; Bearpark, M.; Heyd, J. J.; Brothers, E.; Kudin, K. N.; Staroverov, V. N.; Kobayashi, R.; Normand, J.; Raghavachari, K.; Rendell, A.; Burant, J. C.; Iyengar, S. S.; Tomasi, J.; Cossi, M.; Rega, N.; Millam, N. J.; Klene, M.; Knox, J. E.; Cross, J. B.; Bakken, V.; Adamo, C.; Jaramillo, J.; Gomperts, R.; Stratmann, R. E.; Yazyev, O.; Austin, A. J.; Cammi, R.; Pomelli, C.; Ochterski, J. W.; Martin, R. L.; Morokuma, K.; Zakrzewski, V. G.; Voth, G. A.; Salvador, P.; Dannenberg, J. J.; Dapprich, S.; Daniels, A. D.; Farkas, Ö.; Foresman, J. B.; Ortiz, J. V.; Cioslowski, J.; Fox, D. J. *Gaussian 09*, revision A.1, Gaussian, Inc.: Wallingford CT, 2009.
(20) Cossi, M.; Scalmani, G.; Rega, N.; Barone, V. *J. Chem. Phys.* **2002**, *117*, 43–54.
(21) Gonzales, C.; Schlegel, H. B. *J. Phys. Chem.* **1990**, *94*, 5523–5527.
(22) Moller, C.; Plesset, M. S. *Phys. Rev.* **1934**, *46*, 618–622.
(23) Reed, A. E.; Curtiss, L. A.; Weinhold, F. *Chem. Rev.* **1988**, *88*, 899–926.
(24) Becke, A. D. *J. Chem. Phys.* **1993**, *98*, 5648–52.
(25) Boese, A. D.; Martin, J. M. L. *J. Chem. Phys.* **2004**, *121*, 3405–3416.
(26) Zheng, J.; Zhao, Y.; Truhlar, D. G. *J. Chem. Theory Comput.* **2007**, *3*, 569–582.
(27) Radi, R.; Beckman, J. S.; Bush, K. M.; Freeman, B. A. *J. Biol. Chem.* **1991**, *266*, 4244–4250.
(28) Winterbourn, C.; Metodiewa, D. *Free Rad. Med.* **1999**, *27*, 322–328.
(29) Cardey, B.; Enescu, M. *ChemPhysChem* **2005**, *6*, 1175–1180.
(30) Chance, M. R.; Sagi, I.; Wirt, M. D.; Frisbie, S. M.; Scheuring, E.; Chen, E.; Bess, J. W., Jr.; Henderson, L. E.; Arthur, L. O.; South, T. L.; Perez-Alvarado, G. A.; Summers, M. F. *Proc. Natl. Acad. Sci. U.S.A.* **1992**, *89*, 10041–10045.
(31) Clark-Baldwin, K.; Tierney, D. L.; Govindaswamy, N.; Gruff, E. S.; Kim, C.; Berg, J.; Koch, S. A.; Penner-Hahn, J. E. *J. Am. Chem. Soc.* **1998**, *120*, 8401–8409.
(32) Sénéque, O.; Latour, J.-M. *J. Am. Chem. Soc.* **2010**, *132*, 17760–17774.
(33) Fabris, D.; Hathout, Y.; C. Fenselau, C. *Inorg. Chem.* **1999**, *38*, 1322–1325.
(34) Maynard, A. T.; Covell, D. G. *J. Am. Chem. Soc.* **2001**, *123*, 1047–1058.
(35) Tahir Ali, S; Karamat, S.; Kóňa, J.; Fabian, W. M. F. *J. Phys. Chem. A* **2010**, *114*, 12470–12478.
(36) Wilker, J. J.; Lippard, S. J. *Inorg. Chem.* **1997**, *36*, 369–378.
(37) Cardey, B.; Enescu, M. *J. Phys. Chem.* **2007**, *111*, 673–678.